Cells Tissues Organs

Cells Tissues Organs 2005;180:44–53
DOI: 10.1159/000086198

Anatomically Based Modelling of the Human Skull and Jaw

N.L. van Essen[a] I.A. Anderson[a] P.J. Hunter[a] J.B. Carman[b] R.D. Clarke[c] A.J. Pullan[a]

[a]Bioengineering Institute, The University of Auckland, [b]The University of Auckland, Auckland, [c]AgResearch Ltd., Hamilton, New Zealand

Key Words
Jaw modelling · Finite element method · Mastication

Abstract
We present here an anatomically based model of the human masticatory system that provides a framework for simulating the complex chewing process. The initial motivation for creating this model was the desire to have a computational model of the human jaw that can be used to simulate the action of simple bites, and to calculate the stresses and forces on the teeth that are involved. The model created also provides a platform that can be used to investigate other features of the masticatory system. To construct this global model, individual models of the bones of the skull and jaw were created from generic data sets. Geometric models of the muscles of mastication were also created and attached to the appropriate bones. To complete this initial model, representations of the crowns of the teeth were created and a basic model of the temporomandibular joint (TMJ) was included. The finite element method was used to solve for the stresses and strains created by the loading conditions during a clenching simulation involving the mandible bone. The model presented here is also discussed in relation to a model of the entire musculo-skeletal system being developed as part of the Physiome Project.

Introduction

A properly functioning masticatory system is very important to a person's wellbeing; however, this system is prone to dysfunction, whether with the teeth or with the jaw joints. In order to better deal with these problems it is necessary to have a good understanding of how the masticatory system functions. One possible way to increase this understanding is through the use of mathematical modelling. There are two main mathematical modelling techniques that have been used to study the masticatory system, involving models that focus on the kinematics of the system or models that use numerical techniques such as the finite element method (FEM) to calculate stresses within the components of the system.

Kinematically focused models treat the mandible as a rigid body, with attached muscles modelled as single force vectors. A basic model of the temporomandibular joint (TMJ) is included in such models to constrain the movement of the mandible. The objective of these models is to

Abbreviations used in this paper

FEM	finite element method
RMS	root mean squared
TMJ	temporomandibular joint

KARGER

Fax +41 61 306 12 34
E-Mail karger@karger.ch
www.karger.com

1422–6405/05/1801–0044$22.00/0

Accessible online at:
www.karger.com/cto

Nina van Essen
Bioengineering Institute, Faculty of Engineering
University of Auckland, Private Bag 92019
Auckland (New Zealand)
Tel. +64 9 373 7599, ext. 89742, Fax +64 9 367 7157, E-Mail n.vanessen@auckland.ac.nz

simulate the movement of the mandible by applying suitable muscle forces in the directions of the force vectors. The masticatory system is known to be kinematically indeterminate [Koolstra and van Eijden, 2001], with a particular movement of the mandible able to be produced by a variety of combinations of muscle activations. This means some form of optimisation algorithm must be used to determine muscle functions. The common objective functions used attempt to minimise joint load [Trainor et al., 1994], or total muscle forces [Baragar and Osborn, 1987; Koolstra and van Eijden, 2001]. These kinematically focused mathematical models are primarily used to study the movement of the mandible and how this is influenced by actions of muscles; however, they cannot be used to calculate stresses within bones.

Some models of the masticatory system geometry use the finite element method to solve for the stresses and strains created by loading conditions. Many of these finite element models only focus on very specific regions, most notably the TMJ. Early finite element models of the TMJ were two-dimensional [Chen and Xu, 1994; Chen et al., 1998]; however, recently there have been some three-dimensional models [e.g. Nagahara et al., 1999; Beek et al., 2000, 2001; Tanaka et al., 2001, 2004; del Pozo et al., 2003; Donzelli et al., 2004]. These models focus on the movement and stresses on the TMJ disc and articular surfaces during jaw opening and clenching. There has also been some work using finite element models of the full jaw by Korioth et al. [1992], Korioth and Hannam [1994], and Hu et al. [2003]. These studies analysed the stresses and linear elastic deformation in the mandible during clenching simulations.

The purpose of this paper is to present a new anatomically realistic generic computational model of the entire human skull and jaw that uses the finite element method to calculate stresses and displacements of the masticatory system components. This model differs from previous finite element models in a number of ways. The geometry of this skull and jaw model was created using high order cubic Hermite elements rather than linear elements. These elements preserve the derivative continuity between element boundaries, allowing for a mesh that accurately represents the geometry using a far smaller number of elements than a linear mesh. A description of cubic Hermite interpolation is given in Appendix 1. Our model has also been designed to offer more flexibility of application than any models previously created. To achieve this, models of the full geometry of the skull bones, plus the muscles involved in mastication have been created. Although the model has currently only been used in a static clenching simulation involving the mandible it will be capable of solving simulations of movements involved in mastication.

Methods

Model Creation

The geometry of the jaw model was obtained from several sources of data. The bone data were digitised from a set of anatomically accurate drawings of an averaged adult Caucasian male skull. Details of these drawings are given in Appendix 2. This set of bone data was used in order to create a generic skull and jaw model, making it a good starting point for creating customised models for different individuals if necessary.

To construct our mesh using cubic Hermite elements, we formulated it as an optimisation problem, as described in Fernandez et al. [2004]. An iterative linear fitting algorithm was used as follows. Firstly an initial mesh was created by choosing some of the data points as nodes that were used for producing linear elements. The data points were then projected onto the flat mesh surfaces to obtain the root mean squared (RMS) error of the distance separating the mesh surface from all the data points. The optimisation problem was then solved and nodal positions and derivatives of the mesh were adjusted so that the element surfaces deformed and moved closer to the data points (to 'fit' the data). The data points were then re-projected onto the deformed mesh and the new error was calculated. This procedure of error estimation, optimisation problem solution and mesh updating was repeated until the error was within some desired value. The mesh creation procedure is illustrated in figure 1.

Since no generic data were available to us on the teeth, the data used to create the tooth models came from a scan of the surfaces of the crowns of a given individual. Due to the limited data, and to keep the model from becoming overly complex at this early stage, only the crowns of the teeth were modelled. These initial models were rigidly attached to the bones. This reduced detail was considered to be adequate since the main focus was on global jaw movements and general deformations and stresses throughout the mandible. However, if more detailed stresses are required around the teeth then it is certainly possible to add more detail to the teeth.

The occlusal surfaces of the tooth models were created to approximate the cusps of the teeth, and to fit together with a realistic occlusion as described in anatomy texts [Gray, 1918; McDevitt, 1989; Fehrenbach and Herring, 1996]. The data used for the teeth are shown in figure 2 along with the tooth models attached to the bones.

The muscle data were gathered from the Visible Human project [Spitzer et al., 1996]. The procedure for obtaining the data for our fitting procedure involved stacking slices 5 mm apart in the correct positions, then tracing the outline of the muscles on each slice with a number of data points as shown in figure 3a. This enabled a three-dimensional set of data points for the surface of the entire muscle to be built up, as shown for the temporalis muscle in figure 3b. Data were collected for the suprahyoid muscles as well as for the four pairs of 'muscles of mastication' the masseter, temporalis, medial pterygoid and lateral pterygoid in order to model the muscles involved in all jaw movements. The muscle models were created in a similar manner to the bones using the finite element fitting procedure previously discussed. Finer details of surface geometry and attachment

points were adjusted with guidance from anatomists, and by referring to anatomy texts [Gray, 1918; McGrath and Mills, 1984; McDevitt, 1989; Ellis et al., 1991; Fehrenbach and Herring, 1996]. The final muscle models are shown with the bone mesh in figure 3d, e.

The models that have been created using the above procedure are suitable for a variety of computational simulations. In order to use the model for computational simulations, however, extra detail was required specifying the material properties of components of the model. Exactly what physical process is to be simulated using the model will determine what additional detail is required. If jaw movements involving the muscles deforming or contracting are to be solved then additional detail in the muscle models such as anisotropic elastic data based on fibre directions will be required. However, if stresses and strains in the bone are to be calculated then the material properties of the bone must be included in the model. We describe below our initial work on simulating clenching using the mandible bone only. Since large displacements in the bone typically do not occur, at the continuum level the bone is assumed to behave as a linearly elastic material (as described in Appendix 3). For the linear elasticity simulation the elastic moduli and Poisson's ratio of the bone were specified.

Bone is primarily made up of two types, cortical and cancellous. The mandible consists of a cancellous bone core surrounded by cortical bone as illustrated in figure 4a. In our clenching simulation both bone types were modelled as isotropic materials as has been done in previous finite element studies. A Young's modulus of 10 GPa was used for the cortical bone. Whilst this value is slightly lower than the 13.7 GPa that has been used in other finite element studies [Chen et al., 1998; Nagahara et al., 1999; Tanaka et al., 2000, 2001, 2004; Hu et al., 2003], it is more in line with the experimental values found in Lettry et al. [2003]. The cancellous bone Young's modulus used in literature varies widely, with the above studies using 7.9 GPa, whereas the finite element model by Korioth and Hannam [1994] used a value of 0.38 GPa. For our simulation a modulus value of 1 GPa was chosen for the value of Young's modulus of cancellous bone. Poisson's ratio used for both bone types was 0.3, with this value being commonly used throughout the literature. Figure 4b shows a cross-section from the body of the mandible model illustrating the cortical and cancellous regions as modelled.

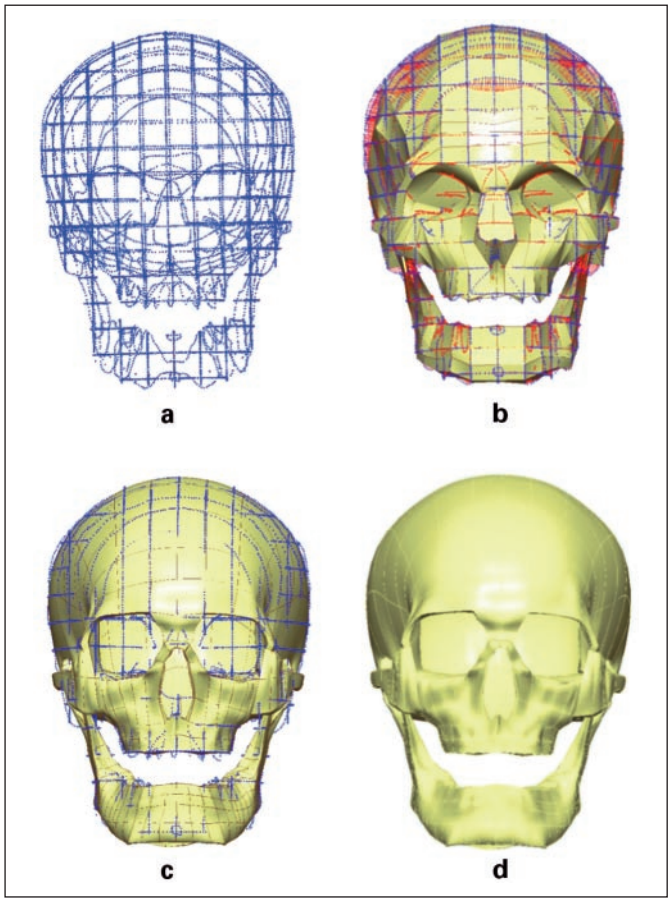

Fig. 1. a The bone data digitised from the skull drawings. **b** An initial linear mesh is created by choosing some of the data points to use as nodes, then joining these up with straight lines to create the elements. The data points are then projected orthogonally onto the initial mesh as shown and the error is calculated, shown by the red lines. The fitting technique is used to adjust the node positions and derivatives to create the curved fitted mesh shown in **c** with the data shown with blue crosses. This process is repeated until the errors are within acceptable limits. The final fitted mesh is shown on its own in **d**.

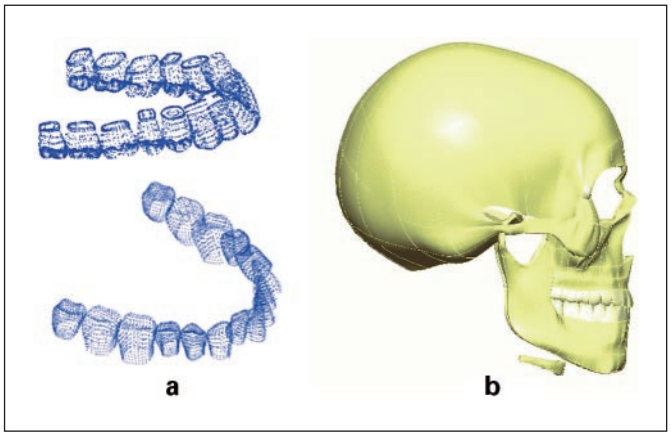

Fig. 2. a Data from the scanned teeth. **b** Bone model with the teeth added.

Fig. 3. a One slice of the visible human data set showing the temporalis muscles outlined with data points. **b** The full data set of the temporalis muscles built up by tracing around the muscle outlines on several slices. The completed data set for all the muscles modelled is shown in **c** where the temporalis data are purple, the masseter data yellow, the medial pterygoid data green, the lateral pterygoid data blue and the data points for all the suprahyoid muscles are red. In **d** the full set of fitted muscle models is shown with the some colours as for the data. The completed jaw geometry including muscles, teeth and bones is shown in **e**.

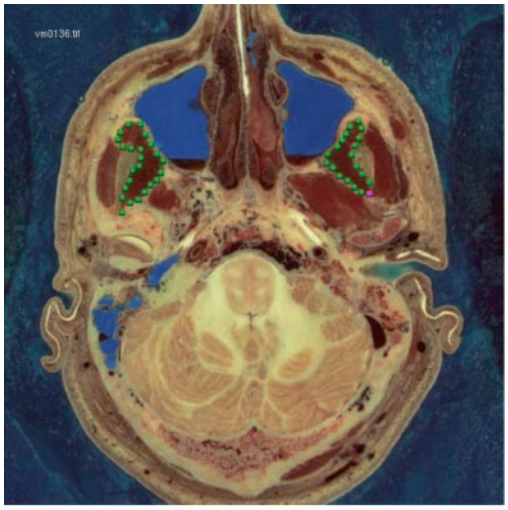

a

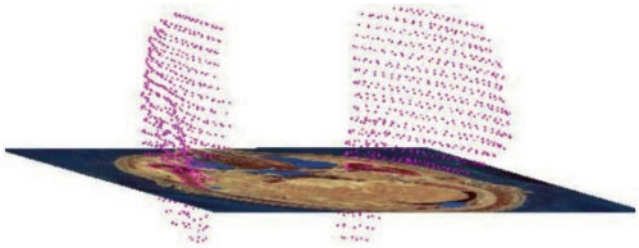

b

c

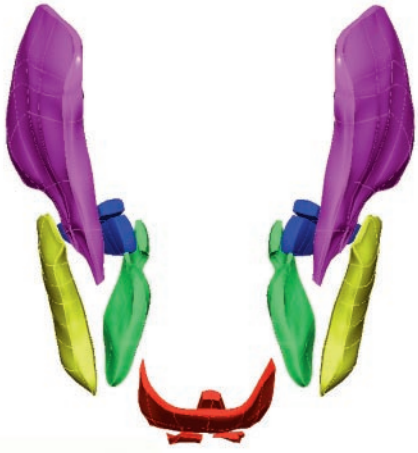

d

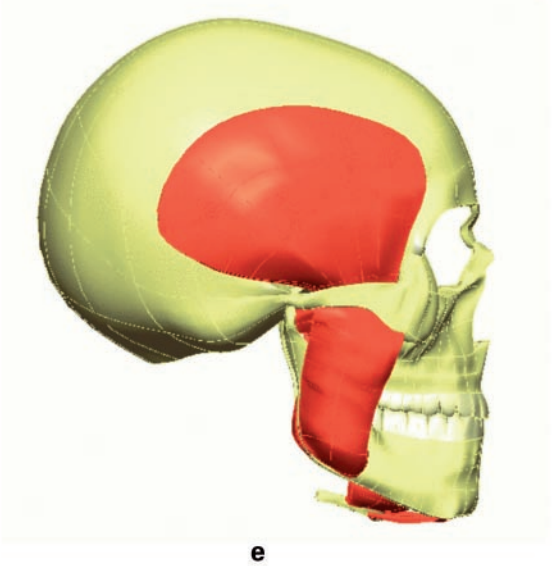

e

3

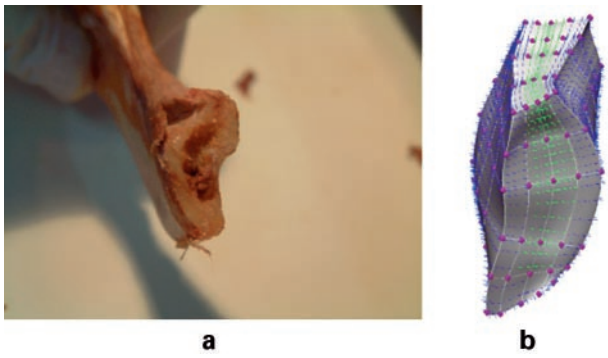

4

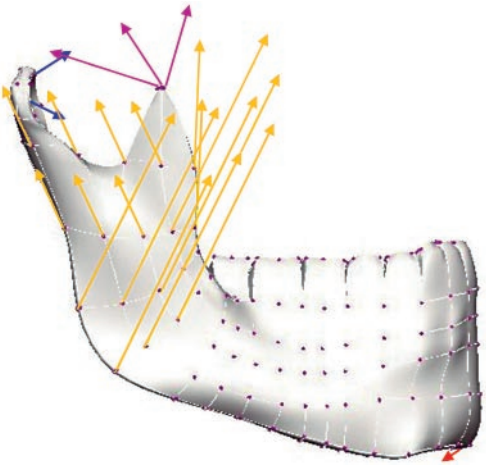

5

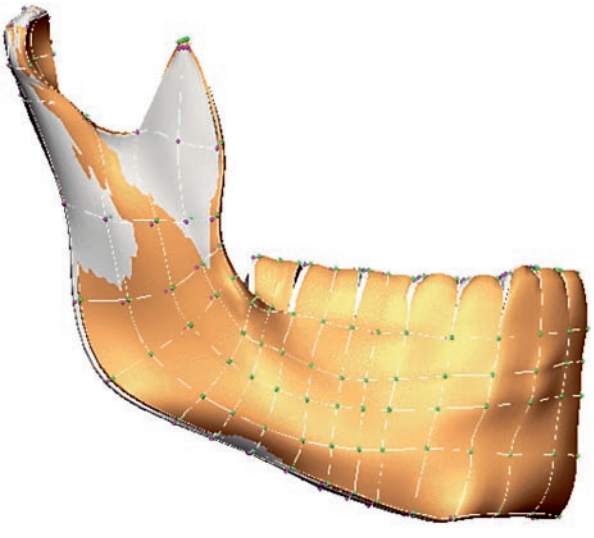

6

Clenching Simulation

In order to create a realistic clenching simulation it was necessary to determine what forces the muscles are applying to the mandible in this state. Force data from a previous finite element study on the mandible by Korioth and Hannam [1994] was used as the basis for the clenching simulation.

The muscle forces were described using unit vectors giving the muscle directions, with weighting and scaling factors indicating the force magnitude. The weighting factor is the total muscle force that could be generated by a particular muscle, with the scaling factor indicating the ratio of that muscle's contraction during the clenching task compared to the maximum. For muscles with wide attachment areas, where the applied force is in more than one direction, more than one unit vector was given. The temporalis muscle, for example, was split into anterior, middle and posterior parts, while the masseter muscle was split into superficial and deep parts. To simulate the muscle forces being applied over wide attachment areas a number of parallel force vectors were used for each muscle. The muscle force data are detailed in table 1. The muscle force magnitudes were obtained by multiplying the weighting factor by the scaling factor [as detailed in Korioth and Hannam, 1994]. The muscle force vectors were then found by scaling the unit vectors by the force magnitudes, and these force vectors were evenly portioned between all the nodes in the muscle's attachment area. Figure 5 illustrates the muscle force vectors acting on the mandible. The displacement boundary conditions for this clenching simulation involved preventing the condyles from translating in any direction to simulate being fixed in the TMJ fossa. The canines, premolars and molars were all prevented from moving vertically or bilaterally.

Results

The accuracy of the fit for the mandible model and the bottom teeth used in the clenching simulation was obtained by projecting the data points onto the final fitted mesh and calculating the RMS error. The RMS error for

Fig. 4. a Cross-section of the mandible showing the cancellous core and surrounding cortical bone. **b** Section of the mandible model illustrating the cancellous and cortical regions as modelled. The green crosses indicate the cancellous regions and the blue crosses the cortical bone region.

Fig. 5. The mandible model with arrows representing the muscle force vectors. The purple arrows indicate the temporalis muscle, the yellow indicates the masseter muscle, the blue indicates the lateral pterygoid muscle and the red the digastric muscle. The medial pterygoid force vectors are not shown as they are acting on the inside of the mandible.

Fig. 6. The mandible model showing initial (white) and deformed (gold) states from the clenching simulation. The actual deformation is shown without exaggeration. The maximum deformation can be seen at the point of the coronoid process, due to the action of the temporalis muscle. The angle of the mandible is also deformed outwards and forwards, due to the strong force provided by the masseter muscle.

Table 1. Muscle force data taken from Korioth and Hannam [1994], adjusted for our model's coordinate system

Muscle	Nodes n	Weighting factor (N)	Scaling factor (L)	Scaling factor (R)	Unit vector (X)	Unit vector (Y)	Unit vector (Z)
Superficial masseter	8	190.4	1.00	1.00	0.207	0.419	0.884
Deep masseter	7	81.6	1.00	1.00	0.546	–0.358	0.758
Medial pterygoid	6	174.8	0.76	0.76	–0.4486	0.373	0.791
Anterior temporalis	6	158.0	0.98	0.98	0.149	0.044	0.988
Middle temporalis	3	95.6	0.96	0.96	0.222	–0.500	0.837
Posterior temporalis	5	75.6	0.94	0.94	0.208	–0.855	0.474
Inferior lateral pterygoid	3	66.9	0.27	0.27	–0.630	0.757	–0.174
Superior lateral pterygoid	3	28.7	0.59	0.59	–0.761	0.645	0.074
Anterior digastric	4	40.0	0.28	0.28	0.244	–0.940	–0.237

The unit vectors are for muscles on the right side and can be adjusted for left muscles by swapping the sign of the X value. The table shows for each of the muscle sections used, the number of nodes included in the attachment area along with the values used to calculate the muscle force vectors. The weighting factor is the total muscle force that can be generated by that muscle section. The scaling factor indicates for the left or right muscle section the ratio of muscle contraction compared to the maximum possible activity. The weighting factor and the scaling factor multiply to give the muscle force magnitude. The force vectors are obtained by multiplying the muscle force magnitudes by the unit vectors for each muscle section.

the mandible model was 1.06 mm, and the error for the tooth models was 0.71 mm.

The calculated displacements in the mandible during the clenching simulation were small, with the maximum displacement being only 0.3 mm. The original and deformed geometry of the mandible is shown in figure 6. The point of maximum displacement was at the top of the coronoid process, with 0.3 mm displacement in the vertical direction. The displacements calculated around the lower jaw border showed that there was an expansion of the mandible mainly around the angle, which reduced towards the front of the jaw. The lower jaw border moved upwards slightly in the same regions. The dental arch also expanded slightly, particularly towards the back molars.

Discussion

We have presented above an extensible modelling framework of the human masticatory system. This model extends the work of previous finite element models that have been created of the jaw with the use of high order elements allowing for the geometry to be represented more realistically than linear elements allow. A static clenching simulation has been performed using the mandible. The results from this simulation indicate that our model is capable of calculating realistic displacements and stresses of the bone caused by the muscle forces. All of the displacements calculated in our clenching simulation match the results from the Korioth and Hannam [1994] study, in terms of directions and the relative displacements of different regions of the model. The position of maximum displacement matched that found in Korioth and Hannam [1994], where the coronoid process had 0.46 mm displacement. The reduced displacement in this model would be expected as the material properties used here differed from those used in Korioth and Hannam [1994] resulting in a stiffer model. These results indicate that one limitation on the accuracy of the model simulations appears to be the bone material properties that are used. For the clenching simulation performed appropriate values for Young's modulus and Poisson's ratio were chosen, with the bone considered to be homogeneous and isotropic. Experimental studies [Huiskes, 1982; Lettry et al., 2003], indicate that cortical bone most closely resembles an orthotropic material. The cortical bone of the mandible has been modelled as orthotropic in a few studies [Hart et al., 1992; Korioth and Hannam, 1994], although it has been more commonly modelled as isotropic [Chen et al., 1998; Nagahara et al., 1999; Tanaka et al., 2000, 2001, 2004; Hu et al., 2003]. If more detailed data of mandible bone material properties could be obtained then our model has the capability of modelling anisotropic materials. The elas-

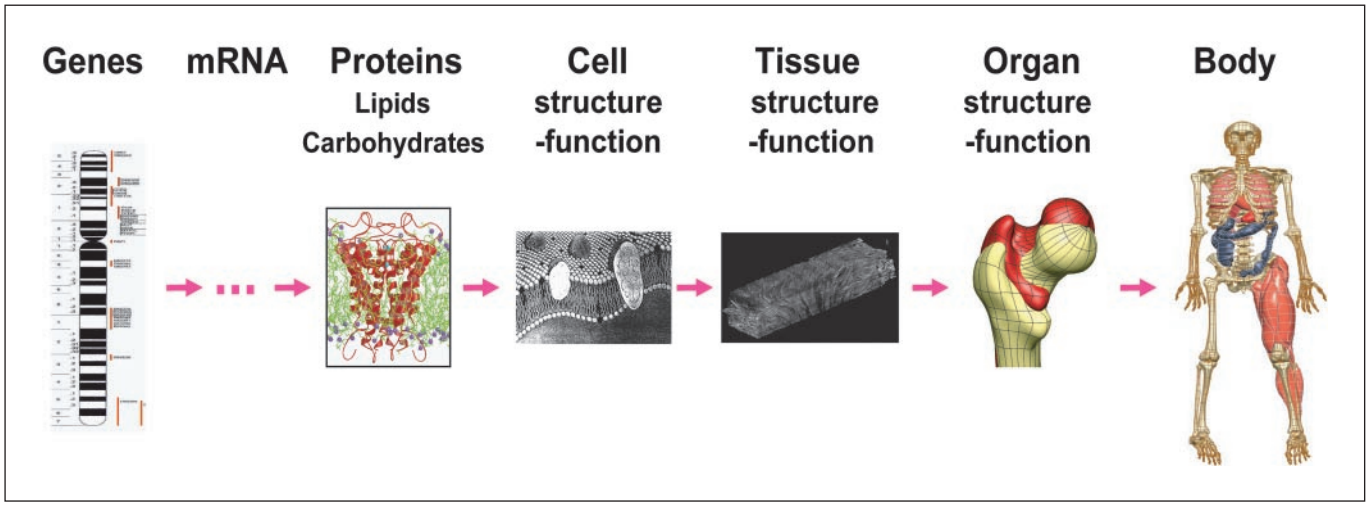

Fig. 7. Understanding physiological function via a multiscale anatomically and biophysically based approach to computational modelling.

tic moduli and Poisson's ratio values can also be specified at discrete positions within the mesh, or interpolated across each element using the cubic Hermite basis functions allowing for the inhomogeneous nature of bone to be taken into account.

The anatomically based models of the jaw and TMJ described above are part of a larger project to model the complete musculo-skeletal system within the framework of the Physiome Project [Hunter and Borg, 2003]. The aim of the Physiome Project is to build models of physiological processes that span multiple spatial scales from genes and proteins to cells, tissues and organs as illustrated in figure 7. At the larger spatial scale of tissues and organs these models are based on continuum physics and use methods similar to those used in the analysis of any engineering structure – except that, unlike most engineering structures, the materials are nonlinear, anisotropic and inhomogenous. As one moves down the spatial scale the equations move from partial differential equations to ordinary differential equations to stochastic systems and network models. The greatest challenges lie in developing models that bridge across the spatial scales.

Summary and Conclusions

We have created a computational modelling framework for studying the function of the masticatory system. Geometrical models of the bones of the skull and jaw have been created, along with models of the muscles involved in mastication. Initial models of the crowns of the teeth have also been included. The mandible model has been used in a simple clenching simulation, the results of which indicate that the model is capable of obtaining realistic stresses and displacements of the bone. Further applications planned for the modelling framework include simulating motion of the mandible, studying the articulation of the TMJ and calculating the stresses in the TMJ disc. In order to achieve this, a detailed model of the TMJ anatomy is to be created. Kinematic data of jaw movement are being collected to use as boundary conditions for the simulation.

Appendix 1: Cubic Hermite Interpolation

The standard one-dimensional linear Lagrange basis functions used for interpolating over the mesh elements are

$$\varphi_1(\xi) = 1 - \xi$$
$$\varphi_2(\xi) = \xi$$

where ξ is a local coordinate on the element (varying from 0 at local node 1 to 1 at local node 2). The linear interpolation formula for this case is

$$\phi(\xi) = \varphi_\alpha(\xi)\,\phi_\alpha \quad (\alpha = 1,2) \quad \equiv \varphi_1(\xi)\phi_1 + \varphi_2(\xi)\,\phi_2$$

where ϕ_a is the value of ϕ at node α. This type of interpolation preserves continuity between elements, but does not preserve slope continuity. This interpolation can be extended to two or three dimensions by using a local ξ variable in each direction.

In contrast to this, the one-dimensional cubic Hermite basis functions are

$$\Psi_1^0(\xi) = 1 - 3\xi^2 + 2\xi^3;\ \Psi_1^1(\xi) = \xi(\xi-1)^2$$
$$\Psi_2^0(\xi) = \xi^2(3-2\xi);\quad \Psi_2^1(\xi) = \xi^2(\xi-1)$$

The interpolation formula for this case is

$$\phi(\xi) = \Psi_\alpha^i(\xi)\,\phi_{,i}^\alpha \qquad (i = 0,1;\ \alpha = 1,2)$$
$$\equiv \Psi_1^0(\xi)\,\phi_1 + \Psi_1^1(\xi)\left.\frac{\partial\phi}{\partial\xi}\right|_1 + \Psi_2^0(\xi)\,\phi_2 + \Psi_2^1(\xi)\left.\frac{\partial\phi}{\partial\xi}\right|_2$$

where

$$\phi_{,0}^\alpha$$

is the value of ϕ at node α and

$$\phi_{,1}^\alpha = \frac{\partial\phi}{\partial\xi}$$

at node α, α = 1,2. This interpolation expression preserves both continuity of function and derivative across element boundaries.

A two-dimensional bicubic Hermite basis requires three derivatives per node, a derivative of ϕ with respect to each of the ε directions plus a cross-derivative. The bicubic interpolation of these nodal parameters is given by

$$\begin{aligned}\phi(\xi_1,\xi_2) = {} & \Psi_1^0(\xi_1)\Psi_1^0(\xi_2)\,\phi_1 + \Psi_2^0(\xi_1)\,\Psi_1^0(\xi_2)\,\phi_2 + \\ & \Psi_1^0(\xi_1)\Psi_2^0(\xi_2)\,\phi_3 + \Psi_2^0(\xi_1)\Psi_2^0(\xi_2)\,\phi_4 + \\ & \Psi_1^1(\xi_1)\Psi_1^0(\xi_2)\left.\frac{\partial\phi}{\partial\xi_1}\right|_1 + \Psi_2^1(\xi_1)\Psi_1^0(\xi_2)\left.\frac{\partial\phi}{\partial\xi_1}\right|_2 + \\ & \Psi_1^1(\xi_1)\Psi_2^0(\xi_2)\left.\frac{\partial\phi}{\partial\xi_1}\right|_3 + \Psi_2^1(\xi_1)\Psi_2^0(\xi_2)\left.\frac{\partial\phi}{\partial\xi_1}\right|_4 + \\ & \Psi_1^0(\xi_1)\Psi_1^1(\xi_2)\left.\frac{\partial\phi}{\partial\xi_2}\right|_1 + \Psi_2^0(\xi_1)\Psi_1^1(\xi_2)\left.\frac{\partial\phi}{\partial\xi_2}\right|_2 + \\ & \Psi_1^0(\xi_1)\Psi_2^1(\xi_2)\left.\frac{\partial\phi}{\partial\xi_2}\right|_3 + \Psi_2^0(\xi_1)\Psi_2^1(\xi_2)\left.\frac{\partial\phi}{\partial\xi_2}\right|_4 + \\ & \Psi_1^1(\xi_1)\Psi_1^1(\xi_2)\left.\frac{\partial^2\phi}{\partial\xi_1\partial\xi_2}\right|_1 + \Psi_2^1(\xi_1)\Psi_1^1(\xi_2)\left.\frac{\partial^2\phi}{\partial\xi_1\partial\xi_2}\right|_2 + \\ & \Psi_1^1(\xi_1)\Psi_2^1(\xi_2)\left.\frac{\partial^2\phi}{\partial\xi_1\partial\xi_2}\right|_3 + \Psi_2^1(\xi_1)\Psi_2^1(\xi_2)\left.\frac{\partial^2\phi}{\partial\xi_1\partial\xi_2}\right|_4\end{aligned}$$

Further details on the cubic Hermite basis functions can be found in Bradley et al. [1997].

Appendix 2: Skull Data

The bone model used in this study is based on three orthogonally oriented maps of fully reconciled closely spaced contours of the free surfaces of a hypothetical normalized human skull and mandible. Key anthropometric points to control size and general shape were derived from data from 1,000 male skulls from 17 ethnic groups which provided unweighted means for 55 point-to-point distances [Howells, 1973]. These data were converted to points in a Cartesian coordinate system with its defining axis in the plane of symmetry and parallel to the Frankfort horizontal plane. Principal cranial contours were refined using data from 112 male skulls from Hythe [Stoessiger and Morant, 1932] and more specific studies [Young, 1957; Olivier, 1974]. Sagittal facial form was refined using data on the bony nasopharynx [Bergland, 1963] and mandibular form from data from 102 twenty-to-thirty year-olds [Solow, 1966]. Key points on the sphenoid bone were derived from data from some 800 Egyptian male skulls (Series E) [Woo, 1931; Pearson and Woo, 1935]. Many details were based on data from Lang [1983].

Contours were then generated at 5-mm intervals using cross-sectional data from atlases [for instance, Maue-Dickson et al, 1983; McGrath and Mills, 1984] and specially prepared anatomical material. In each specific region the contour in one of the orthogonal planes was usually characteristic and easily fitted in relation to two or more of the established anthropometric points. Sections in the two other planes were systematically fitted and checked against sectional material, the contours in all three planes being carefully refined and reconciled until they all matched available data closely. The aim throughout was to have each contour capture the qualitative features shared by several examples from sectioned material while conforming to the constraints on size and orientation established by the anthropometric data. The contours (fig. 8) are those of a representative standard skull and the finite element model was fitted to this virtual skull.

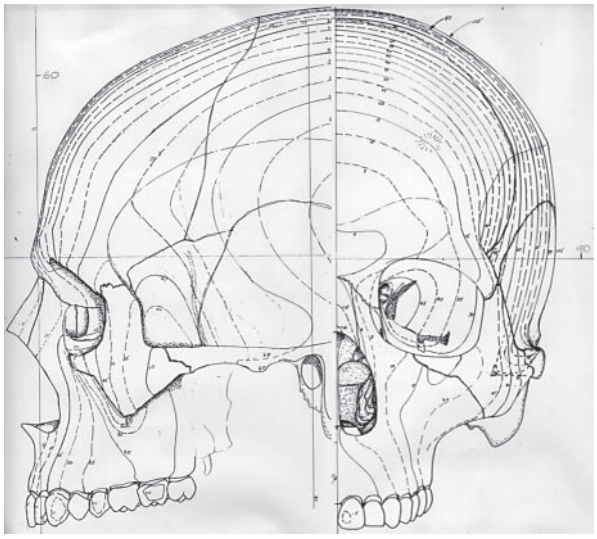

Fig. 8. Contours from some of the skull drawings that the bone data were obtained from.

Appendix 3: Linear Elasticity Equations

If a body is in equilibrium then we have

$$\sigma_{ij,j} + b_i = 0 \qquad (i,j = 1,2,3) \tag{1}$$

where σ_{ij} are the components of the stress tensor and b_i is the body force per unit volume. Also note that

$$\sigma_{ij,j} = \frac{\partial \sigma_{ij}}{\partial x_j}.$$

For the case of linear elasticity an assumption is made that displacements are small, allowing the small strain tensor to be used

$$e_{ij} = \frac{1}{2}\left(u_{i,j} + u_{j,i} \right) \qquad (i,j = 1,2,3) \tag{2}$$

where u_i and u_j are components of the displacement vector **u**.

The object here is to find the stresses and displacements within the jaw as it is subject to a known set of body forces and prescribed stresses and displacements at the boundary. Given this objective there are 15 unknown quantities to solve for (6 stresses, 6 strains and 3 displacements). There are only 9 equations given in (1) and (2) above, however, which are not sufficient to solve for all the unknowns. Therefore an extra set of equations is required. These are the material-dependent constitutive laws which define the stress-strain relationships of a particular material.

$$\sigma_{ij} = c_{ijkl} e_{kl}$$

where c_{ijkl} are the 81 components of a 4th-order tensor. The number of components can be reduced when there is symmetry of stress-strain behaviour within the material. The simplest material type is isotropic, where the material response is the same in every direction. In this case the constitutive law simplifies to the generalised Hooke's law

$$\sigma_{ij} = \lambda e_{kk} + 2\mu e_{ij} \tag{3}$$

where λ, μ are Lamé's constants. Two material properties must be specified for these constitutive equations, Young's modulus E and Poisson's ratio υ. These are related to Lamé's constants by

$$E = \frac{\mu(3\lambda + 2\mu)}{\lambda + \mu}$$

$$\upsilon = \frac{\lambda}{2(\lambda + \mu)}$$

Providing the displacements are continuous functions of position then the equations 1, 2 and 3 are sufficient to determine the 15 unknowns.

References

Baragar, F.A., J.W. Osborn (1987) Efficiency as a predictor of human jaw design in the sagittal plane. J Biomech *20:* 447–457.

Beek, M., J.H. Koolstra, L.J. van Ruijven, T.M.G.J. van Eijden (2000) Three-dimensional finite element analysis of the human temporomandibular joint disc. J Biomech *22:* 307–316.

Beek, M., J.H. Koolstra, L.J. van Ruijven, T.M.G.J. van Eijden (2001) Three-dimensional finite element analysis of the cartilaginous structures in the human temporomandibular joint. J Dent Res *80:* 1913–1918.

Bergland, O. (1963) The bony nasopharynx. A roentgen-craniometric study. Acta Odont Scand 21 (suppl 35).

Bradley, C.P., A.J. Pullan, P.J. Hunter (1997) Geometric modelling of the human torso using cubic Hermite elements. Ann Biomed Eng *25:* 96–111.

Chen, J., U. Akyuz, L. Xu, R.M.V. Pidaparti (1998) Stress analysis of the human temporomandibular joint. Med Eng Phys *20:* 565–572.

Chen, J., L. Xu (1994) A finite element analysis of the human temporomandibular joint. J Biomech Eng *116:* 401–407.

del Pozo, R., E. Tanaka, M. Tanaka, et al. (2003) Influence of friction at articular surfaces of the temporomandibular joint on stresses in the articular disk: a theoretical approach with the finite element method. Angle Orthod *73:* 319–327.

Donzelli, P.S., L.M. Gallo, R.L. Spilker, S. Palla (2004) Biphasic finite element simulation of the TMJ disc from in vivo kinematic and geometric measurements. J Biomech (in press).

Ellis, H., B. Logan, A. Dixon (1991) Human cross-sectional anatomy: atlas of body sections and CT images. Oxford, Butterworth-Heinemann.

Fehrenbach, M.J., S.W. Herring (1996) Illustrated anatomy of the head and neck. Philadelphia, Saunders.

Fernandez, J.W., P. Mithraratne, S.F. Thrupp, et al. (2004) Anatomically based geometric modelling of the musculo-skeletal system and other organs. Biomech Model Mechanobiol *2:* 139–155.

Gray, H. (1918) Anatomy of the human body. Philadelphia, Lea & Febiger.

Hart, R.T., V.H. Vincent, N. Thongpreda et al. (1992) Modeling the biomechanics of the mandible: A three-dimensional finite element study. J Biomech *25:* 261–286.

Howells, W.W. (1973) Cranial variations in man. Cambridge, Harvard University.

Hu, K., R. Qiguo, J. Fang, J.J Mao (2003) Effects of condylar fibrocartilage on the biomechanical loading of the human temporomandibular joint in a three-dimensional, nonlinear finite element model. Med Eng Phys *25:* 107–113.

Huiskes, R. (1982) On the modelling of long bones in structural analyses. J Biomech *15:* 65–69.

Hunter, P.J., T.K. Borg (2003) Integration from proteins to organs: The Physiome Project. Nat Rev Mol Cell Biol *4:* 237–243.

Koolstra, J.H., T.M.G.J. van Eijden (2001) A method to predict muscle control in the kinematically and mechanically indeterminate human masticatory system. J Biomech *34:* 1179–1188.

Korioth, T.W.P., A.G. Hannam (1994) Deformation of the human mandible during simulated tooth clenching. J Dent Res *73:* 56–66.

Korioth, T.W.P., D.P. Romilly, A.G. Hannam (1992) Three-dimensional finite element stress analysis of the dentate human mandible. Am J Phys Anthropol *88:* 69–96.

Lang, J. (1983) Clinical anatomy of the head: Neurocranium, orbit and craniocervical regions. Berlin, Springer.

Lettry, S., B.B. Seedhom, E. Berry, M. Cuppone (2003) Quality assessment of the cortical bone of the human mandible. Bone *32:* 35–44.

Maue-Dickson, W., D.R. Dickson, F.W. Pullen (1983) Computed tomographic atlas of the head and neck. Boston, Little, Brown.

McDevitt, W.E. (1989) Functional anatomy of the masticatory system. London, Boston, Wright.

McGrath, P., P. Mills (1984) Atlas of Sectional Anatomy: Head, Neck and Trunk. New York, Karger.

Nagahara, K., S. Murata, S. Nakamura, T. Tsuchiya (1999) Displacement and stress distribution in the temporomandibular joint during clenching. Angle Orthod *69:* 272–279.

Olivier, G. (1974) Biométrie du frontal. Bull All Anat *58:* 25.
Pearson, K, T.L. Woo (1935) Further investigation of the morphometric characters of the individual bones of the human skull. Biometrika *27:* 424–465.
Solow, B. (1966) The pattern of craniofacial associations. Acta Odont Scand *24* (suppl 46).
Spitzer, V., M.J. Ackerman, A.L. Scherzinger, R.M. Whitlock (1996) The visible human male: A technical report. J Am Med Inform Assoc *3:* 119–130.
Stoessiger, B.N., G.M. Morant (1932) A study of the crania in the vaulted ambulatory of Saint Leonard's church, Hythe. Biometrika *24:* 135–202.
Tanaka, E., R. del Pozo, M. Tanaka, et al. (2004) Three-dimensional finite element analysis of human temporomandibular joint with and without disc displacement during jaw opening. Med Eng Phys *26:* 503–511.
Tanaka, E., D.P. Rodrigo, Y. Miyawaki, et al. (2000) Stress distribution in the temporomandibular joint affected by anterior disc displacement: a three-dimensional analytic approach with the finite-element method. J Oral Rehab *27:* 754–759.
Tanaka, E., D.P. Rodrigo, M. Tanaka, et al. (2001) Stress analysis in the TMJ during jaw opening by use of a three-dimensional finite element model based on magnetic resonance images. Int J Oral Maxillofac Surg *30:* 421–430.
Trainor, P.G.S., K.R. McLachlan, W.D. McCall (1994) Modelling of forces in the human masticatory system with optimization of the angulations of the joint loads. J Biomech *28:* 829–843.
Woo, T.L. (1931) On the asymmetry of the human skull. Biometrika *22:* 324–352.
Young, R.W. (1957) Postnatal growth of the frontal and parietal bones in white males. Am J Phys Anthrop *15:* 367–386.